Article

Dissipative Quantum Criticality as a Source of Strange Metal Behavior

Marco Grilli [1,2], Carlo Di Castro [1], Giovanni Mirarchi [1], Götz Seibold [3] and Sergio Caprara [1,2,*]

1   Dipartimento di Fisica, Università di Roma "La Sapienza", Piazzale Aldo Moro 5, I-00185 Roma, Italy
2   ISC-CNR, Unità di Roma Sapienza, Via dei Taurini 19, I-00185 Roma, Italy
3   Institut für Physik, BTU Cottbus-Senftenberg-PBox 101344, D-03013 Cottbus, Germany
*   Correspondence: sergio.caprara@uniroma1.it; Tel.: +39-06-49914294

Abstract: The strange metal behavior, usually characterized by a linear-in-temperature (T) resistivity, is a still unsolved mystery in solid-state physics. It is often associated with the proximity to a quantum critical point (a second order transition at temperature $T = 0$, leading to a broken symmetry phase) focusing on the related divergent order parameter correlation length. Here, we propose a paradigmatic shift, focusing on a divergent characteristic time scale due to a divergent dissipation acting on the fluctuating critical modes while their correlation length stays finite. To achieve a divergent dissipation, we propose a mechanism based on the coupling between a local order parameter fluctuation and electron density diffusive modes that accounts both for the linear-in-T resistivity and for the logarithmic specific heat versus temperature ratio $C_V/T \sim \log(1/T)$, down to low temperatures.

Keywords: strange metal behavior; cuprates; charge density fluctuations; diffusive modes

1. Introduction

Although the metallic state is usually well described by Landau's Fermi Liquid (FL) theory, there are many systems in which the metallic properties are anomalous, with extended regions of their phase diagram displaying a strange metal behavior [1–4]. The most well-known examples occur in heavy fermion systems in the proximity of quantum critical points (QCPs), i.e., near zero-temperature second-order phase transitions, where the uniform metallic state is unstable towards some ordered state for some critical value x_c of a tuning parameter x, or in high-temperature superconducting cuprates above the optimal superconducting critical temperature (see, e.g., Refs. [5,6], and references therein). More recent examples are found in iron-based superconductors [7] and twisted bilayer graphene [8]. The most prominent feature of the strange metal behavior is a linear-in-T resistivity without any saturation, as a function of the temperature T, up to the highest temperatures. This behavior often starts in the vicinity of a QCP and when the order parameter fluctuations (OPFs) have a two-dimensional (2D) character and the dynamical index is $z = 2$ also a logarithmic C_V/T ratio (C_V being the specific heat) [9,10] is observed, while other power-laws occur when fluctuations are three-dimensional (3D) [2]. In this work, we will focus on quasi-2D systems like cuprates or pnictides and discuss the role of dimensionality in the concluding remarks, Section 5.

Although some theories for the violation of the FL behavior do not rely on an underlying criticality [11–15], the most common interpretations of the strange metal behavior rest on the idea that abundant OPFs in the quantum critical region $x \approx x_c$ may be sufficient to mediate strong effective interactions that spoil the Landau quasiparticle stability and create the non-FL state [16]. This scenario can be realized in different ways, depending on the nature of the ordered phase, which can be antiferromagnetic [17–19], charge density wave [20], nematic [19,21], loop-current [22], or can have a local character [23–25].

We rely on the frustrated phase separation theory for charge density waves in cuprates [20,26–28], where charge density waves are the result of the competition between short- and long-range electron-electron interactions in a strongly correlated electron system, making the FL unstable when the doping-tuned carrier density is reduced below a (temperature-dependent) critical value. The critical line in the temperature T vs. doping p phase diagram ends, at $T = 0$, into a QCP. Due to the strongly anisotropic character of cuprates, the related OPFs in the disordered (FL metallic) phase mostly have a 2D character, and the crossover to a 3D behavior is only achieved at sufficiently low temperatures [26], allowing for the occurrence of a 3D charge-density-wave ordered state that establishes underneath a dome-shaped curve (see, e.g., Ref. [27] and references therein) below a critical doping p_c, which was observed to be $p_c \approx 0.16$ in $YBa_2Cu_3O_y$ [29]. This value is lower than the doping $p^* \approx 0.19$ where the T-linear resistivity extends down to the lowest temperatures when superconductivity is suppressed by strong magnetic fields [5]. Recent resonant inelastic X-ray scattering experiment [30], besides the expected fluctuating nearly-critical charge density waves, associated with the 3D ordered phase, also showed the presence of much shorter-ranged charge density fluctuations (CDFs). These may be the remnant of OPFs of a missed 2D criticality [31], coexisting with nearly-critical fluctuations related to the nearby ordered state.

In a previous work [32], we showed that the observed CDFs in cuprates have a low enough characteristic energy E to be semiclassical in character (i.e., the Bose function ruling their statistics can be approximated by T/E) and are local enough (i.e., they involve a sufficiently broad range of momenta) to account for nearly isotropic scattering as phenomenologically required by the Marginal Fermi Liquid theory [33]. These two ingredients are enough to account for the linear-in-T resistivity observed slightly above optimal doping. We point out that the low energy (smaller than T) and abundance of OPFs in the proximity of a QCP are brought about by the electron-electron interactions driving the FL unstable and by the low dimensionality of the system. We shift our focus from a diverging correlation length to an increasing dissipation that renders the OPFs slower and slower, thereby extending strange metallicity down to lower and lower temperatures. The paradigmatic shift we propose faces a theoretical difficulty of non-FL theories based on the proximity to a QCP characterized by OPFs with a finite characteristic wave vector Q_c. In such theories, the scattering is extremely anisotropic on the Fermi surface, and the FL character of the quasiparticles is spoiled only at isolated points, the so-called hot spots, while scattering at all other points of the Fermi surface is FL-like at sufficiently low-energy, short-circuiting the non-FL behavior at the hot spots [34]. Our proposal was shown to lead to isotropic marginal-FL behavior [32] and the effect that the scattering stays isotropic at the Fermi surface while the scatterer acquires sufficiently low energy to give rise to an extended linear-in-T resistivity.

In subsequent work [35,36], we found that a large dissipation of the OPFs may extend the regime of their semiclassical behavior, thereby accounting for a linear-in-T resistivity down to the lowest temperatures and for the logarithmic divergence of the C_V/T ratio, as it is observed in cuprates at $p \sim p^* > p_c$, when superconductivity is suppressed by high magnetic fields [5]. Nevertheless, the relevant question remained open about the microscopic mechanisms inducing the required dissipation increase.

The motivation of the present work is precisely to provide a possible solution to this last question. Our idea is that the results of this work can somehow fill the gap that was left open in our previous works [35,36], namely the origin of the strong increase in the characteristic relaxation time of OPFs. The explanation we are going to propose gives a central role to the coupling between the OPFs and the diffusion modes of electrons in two dimensions. The present result strongly supports our previous phenomenological assumption of a logarithmic increase in dissipation.

The structure of the paper is the following. In Section 2, we introduce a model for the coupling of OPFs and electron density diffusive modes that are simple enough to be exactly solvable and yet include all the main physical ingredients leading to an enhancement of

damping of the OPFs due to the coupling to other degrees of freedom. In Sections 3 and 4, respectively, we discuss the specific heat and resistivity of cuprates from the point of view of our scenario. Our concluding remarks are found in Section 5.

2. The Order Parameter Fluctuations-Diffusive Modes Model

Taking the CDFs observed in cuprates [30] as a paradigmatic example in which the forthcoming assumptions follow from a description of the experimental data, we consider a regime in which the OPFs have a rather short correlation length, $\xi/\lambda \sim 1-2$ (λ is their characteristic wavelength), by requiring that the system is at a finite distance from the QCP on the disordered side, i.e., at a doping p sufficiently larger than the critical value p_c. In this regime, the fluctuations are largely independent of each other and have a nearly-local character so that they can be represented by a local field at the origin, $\Phi(\mathbf{R} = 0)$. Accordingly, the propagator of these fluctuations has the typical form of an overdamped oscillator

$$\mathcal{D}_0(\omega_n) = (M + \gamma|\omega_n|)^{-1},\tag{1}$$

where ω_n is the boson Matsubara frequency, γ is a dimensionless parameter measuring the damping strength due to the decay of the OPFs into particle-hole (p–h) pairs (Landau damping), the energy scale $M = \nu\xi^{-2}$ stays finite, and ν is an electron energy scale (we adopt units such that the Planck constant $\hbar$ and the Boltzmann constant k_B are set equal to 1, so that angular frequencies, energies, and temperatures have the same units). By analytically continuing to real frequencies, $i\omega_n \to \omega + i0^+$, one can obtain the spectral density of the OPFs, which is broad and peaked at $\omega \approx M/\gamma$, as depicted in Figure 1a.
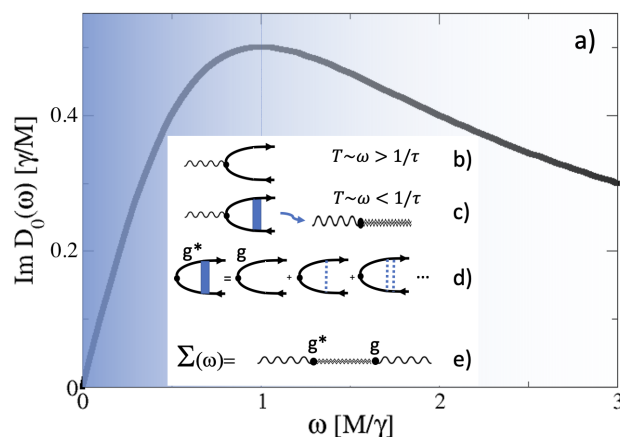

Figure 1. (**a**) Spectral density of the OPF propagator [for the frequency units M/γ see Equation (1)] and a sketch of the coupling (**b**–**d**) between the OPFs (wavy lines) and the p–h diffusive modes (zigzag lines). The solid dots represent their effective coupling g entering Equation (3). (**b**) The high-energy regime in which the OPF decays into a ballistic p–h pair; (**c**) low-energy regime in which the OPF decays into a diffusive p–h pair. The blue rectangle represents the ladder resummation of elastic scattering on quenched impurities represented by dotted lines in (**d**); (**e**) self-energy diagram for the exact solution of the model.

Depending on the typical energy M/γ of the decaying fluctuation, the particle, and the hole can propagate as ballistic particles when their energy (of order M/γ) is larger than $1/\tau$, the elastic scattering rate of the charge carriers on quenched impurities [Figure 1b]. On the other hand, when the fluctuation has lower energy, $M/\gamma < 1/\tau$, a new decay channel opens, with electrons having a diffusive character, as long as $T < 1/\tau$ (for $T > 1/\tau$ the electrons and the holes are in a quasi-ballistic regime, but the OPFs may remain in a classical regime). For $M/\gamma < 1/\tau$, the nearly-local OPF may decay into a p–h diffusive mode [Figure 1c]. We show that this diffusive decay channel of the OPFs triggers the growth of γ and the strange metal behavior is extended down to the lowest temperatures alongside a low-temperature logarithmic growth of the specific heat ratio C_V/T is achieved.

In the standard theory of disordered electron systems [37], a diffusive collective mode is obtained by a ladder resummation of impurity scattering events [the dotted lines in Figure 1d], so that the density–density response function takes the form of a diffusive pole

$$\chi(\mathbf{q}, \omega_n) = \langle \rho(\mathbf{q}, \omega_n) \rho(-\mathbf{q}, \omega_n) \rangle = \frac{N_0 D q^2}{D q^2 + |\omega_n|}, \tag{2}$$

where $\mathbf{q}$ is the wave vector, $q \equiv |\mathbf{q}|$, D is the diffusion constant, and N_0 the quasiparticle density of states at the Fermi level. These density fluctuations keep their singular diffusive form as long as $D q^2$ is smaller than the elastic scattering rate on quenched impurities $1/\tau$.

It is worth noticing that the diffusive character of the low-energy electronic modes is not a property of strongly disordered systems: any standard Drude metal with (even small) amount of impurities has a finite conductance due to impurity scattering, and the electrons (or quasiparticles) at energy smaller than $1/\tau$ diffuse rather than propagate ballistically. Moreover, many strongly correlated systems, with their (strange) metallic character, always display a non-negligible elastic impurity scattering. Cuprates, for instance, have impurity scattering rates of the order of a few tens of meV, such that $T < 1/\tau$ essentially over the whole phase diagram.

To describe an equilibrium situation, where an OPF decays into diffusing p–h pairs, which in turn form back an OPF, we introduce a phenomenological coupling g between an OPF (centered at $\mathbf{R} = 0$) and the diffusive density fluctuation

$$\mathcal{S}_{coupl} = gT \sum_n \Phi(\mathbf{R} = 0, \omega_n) \sum_{\mathbf{q}} \rho(\mathbf{q}, \omega_n). \tag{3}$$

This simplified model has the advantage of being exactly solvable while keeping all the main ingredients to access the physical scenario of an increasing dissipation of the OPFs, due to the coupling to other degrees of freedom. The coupling between OPFs and diffusive modes dresses the OPF propagator, Equation (1), with the self-energy graphically represented in Figure 1e,

$$\begin{aligned} \Sigma(\omega_n) &= g^2 N_0 \int_{Q_{\min}}^{Q_{\max}} \frac{\mathrm{d}^2 q}{4\pi^2} \frac{D q^2}{D q^2 + |\omega_n|} \\ &= \frac{g^2 N_0}{4\pi D} \int_{\Lambda_{\min}}^{\Lambda_{\max}} \mathrm{d}(D q^2) \left(1 - \frac{|\omega_n|}{D q^2 + |\omega_n|} \right) = \delta M - |\omega_n| \delta \gamma. \end{aligned} \tag{4}$$

As usual, the upper momentum cutoff in the diffusion processes is given by the inverse mean free path $Q_{\max} = \ell^{-1}$, which can then be translated into an energy cutoff for the diffusive modes $\Lambda_{\max} \equiv D Q_{\max}^2 = 1/\tau$. For the lower cutoff, $\Lambda_{\min}$, we will consider two possibilities: (*i*) either it is provided by the temperature T, as long as $T < 1/\tau$, i.e., $\Lambda_{\min} \equiv \min(T, \Lambda_{\max})$, (*ii*) or we set $\Lambda_{\min} = 0$, given that the logarithmic divergence in Equation (4) is anyway cutoff by the term $|\omega_n|$ in the denominator. The first term in Equation (4) is a finite correction to the energy scale M, which is immaterial in the forthcoming discussion. Hereafter, we will examine the two possibilities, (*i*) and (*ii*), for the lower cutoff, showing that the resulting scenario is essentially the same.

In case (*i*), expanding to first order in $|\omega_n|$ the last term in Equation (4), one obtains a correction to the dissipation coefficient γ,

$$\delta \gamma = \gamma - \gamma_0 = A \log \max \left[(\tau T)^{-1}, 1 \right], \tag{5}$$

where γ_0 is the damping coefficient in the absence of coupling to diffusive modes and $A \equiv g^2 N_0 / (4\pi D)$ is a dimensionless effective coupling constant. Therefore, the diffusive channel induces a logarithmic increase in the dissipation parameter γ when T decreases. As it was previously shown [35,36], a logarithmically divergent γ leads to a logarithmic divergence of C_V / T with a finite correlation length ξ.

In case (*ii*), one gets a similar result, but now

$$\delta\gamma = A \log\left[1 + (|\omega_n|\tau)^{-1}\right] \tag{6}$$

depends on the frequency and diverges logarithmically as $|\omega_n| \to 0$. As we shall show in Appendix A, this also leads to a logarithmic divergence of C_V/T.

The above results raise the issue of the role of the nearby QCP. In particular, one can notice that Equations (5) and (6) do not explicitly involve the parameter x tuning the proximity to the QCP (in cuprates, this is the doping level p), nor the correlation length characterizing the OPFs. We, therefore, need to equip our microscopic model with the range in x where the above diffusive decay channel becomes effective. First of all, we consider the condition that, when the OPF has a characteristic energy $M/\gamma_0 > 1/\tau$, it can only decay in ballistic p–h pairs and, therefore, $g = 0$. Since the short-range fluctuations are the 2D precursors of the nearby QCP, the correlation length will increase for x approaching x_c and the decay in diffusive p–h pairs sets in when the tuning parameter of criticality x is such that $\nu\xi^{-2} \approx M_0(x - x_c) < \gamma_0/\tau$, i.e., $x < x_{DMD} \equiv x_c + \gamma_0/(\tau M_0)$ (DMD stands for diffusive mode decoupling). This sets the maximum distance from the QCP above, which $\gamma \approx \gamma_0$. On the other hand, our arguments (nearly-independent OPFs, short correlation length ξ) fail when one approaches the QCP, where the physics is ruled by a diverging correlation length ξ and the standard Hertz–Millis picture [38,39] is recovered. Therefore, we are led to assume that the diffusive modes decouple from the OPFs for $(x_c <) x < x_{QCR}$ (QCR stands for the quantum critical regime), giving rise to a negligible $g \approx 0$. Then, Equation (3) only holds in range $x_{QCR} < x < x_{DMD}$.

We point out that the crossover from this regime to the standard Hertz–Millis criticality is not captured by our simplified description. It definitely requires the inclusion of the self-interaction of OPFs. Furthermore, one can conceive a scenario where the short-ranged OPFs described within our approach coexist with nearly-critical (*à la* Hertz–Millis) fluctuations, and the short-ranged OPFs never become long-ranged. This seems exactly to be what is observed in cuprates, where resonant inelastic X-ray scattering experiment [30] highlighted the coexistence of fluctuating charge density waves and much shorter ranged CDFs that can be interpreted as the remnant of a (missed) 2D criticality [31].

3. The Cuprates: Specific Heat

In the case of cuprates, where a charge density wave QCP occurs near optimal doping, at a critical doping p_c hidden under the superconducting dome [20,26,29], we implement the constraint that $g \neq 0$ only for $p_{QCR} < p < p_{DMD}$, phenomenologically imposing in Equation (5) a doping dependence

$$A(p) \approx \alpha \left[\frac{(p - p_{QCR})(p_{DMD} - p)}{p_{QCR}\, p_{DMD}}\right]^2, \tag{7}$$

for $p_{QCR} < p < p_{DMD}$, and $A(p) = 0$, otherwise, where α is a suitable dimensionless prefactor. In the above interval of p, for $T < T_{DMD} \equiv M/\gamma_0 \equiv \nu\xi^{-2}/\gamma_0 \leq 1/\tau$ the additional diffusive channel is open and γ increases, thus lowering M/γ and extending to lower temperatures the strange metal behavior. Figure 2 describes the behavior of $\gamma(p)$ for various temperatures $T = 10\,\text{K}$, $2\,\text{K}$, and $0.5\,\text{K}$. While the shape arises from the choice of the doping dependence of $A(p)$ in Equation (7), the temperature dependence follows Equation (5), reproducing the logarithmic behavior observed for C_V/T in Refs. [10,40,41] and phenomenologically discussed in Refs. [35,36]. Notice that this logarithmic temperature dependence is, therefore, due to $\delta\gamma$ rather than the logarithmic dependence of the specific heat from the correlation length. Reasonable values of the limiting control parameters, of the coefficient A, of the disorder $1/\tau$ and the temperatures are simply chosen for an easier comparison between $\delta\gamma$ and C_V/T to which it is proportional [35]. It is worth emphasizing that the C_V/T variation is not unique among the cuprates: while it seems to diverge at

a specific doping (or in a quite narrow doping range) in Eu-LSCO and Nd-LSCO [10], it displays a broad maximum in LSCO and Bi-2201 instead [40,41]. This variety of behavior is not limited to specific heat data but corresponds to the possible occurrence of strange metal behavior either in narrow or broad intervals of the tuning parameter [2,42–44].
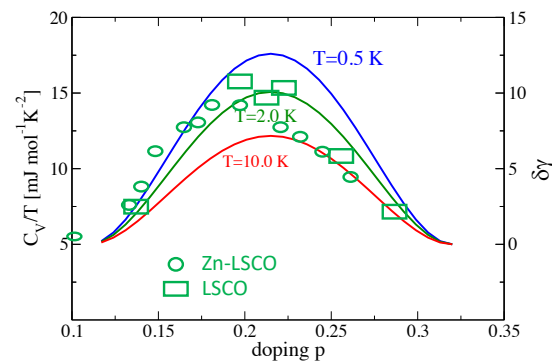

Figure 2. (left y-axis) The green rectangles or circles report the electron-specific heat experimentally measured in $La_{2-x}Sr_xCuO_4$ [40] and Zn-doped $La_{2-x}Sr_xCuO_4$ [41]; (right y-axis) Dissipative parameter correction $\delta\gamma$, Equation (5), for $\alpha = 18.6$, $\frac{1}{\tau} = 500$ K, $p_{QCR} = 0.11$, and $p_{DMD} = 0.32$. These values have been chosen for a closer comparison of the $\delta\gamma$ shape with the specific heat anomaly.

Within the present scenario the doping interval $p_{QCR} < p < p_{DMD}$ is non universal and it can be comparatively broader or narrower in different cuprates, while the relevant non-trivial result is the logarithmic temperature dependence of C_V/T.

4. The Cuprates: Resistivity

Regarding the transport properties, we showed in Ref. [32] that CDFs account for the linear-in-T resistivity in optimally and slightly overdoped YBCO and NBCO samples down to the superconducting critical temperature or slightly above it. The question remained about the linear-in-T resistivity observed for $p \approx p^*$ in strong magnetic fields suppressing superconductivity, which extends down to a few K. Our scenario is summarized in Figure 3. In Figure 3a, we schematically report with red dashed lines the behavior of the CDF characteristic energy at different temperatures $T_1 < T_2 < T_3 < 1/\tau$, both in the ballistic and in the diffusive regimes of their decay. This latter regime occurs when $M/\gamma_0 < 1/\tau$, which defines the doping p_{DMD}. At $T = 0$, within our model, the characteristic energy drops to zero below p_{DMD} due to the logarithmic divergent $\gamma(T)$. For $p < p_{QCR}$, the value of γ is also influenced by the pseudogap, possibly leading to $\gamma < 1$ due to reduced phase space for damping processes. In any case, how M/γ connects to the standard Hertz–Millis QCP is an open issue and, therefore, corresponds to *terra incognita* in Figure 3a. Since typical values for the scattering rates in cuprates are $1/\tau \sim 30$–50 meV, one can notice that the customarily reported phase diagrams of cuprates are usually in the regime where $T < 1/\tau$. Under this condition, we report in Figure 3b a sketch of a cuprate phase diagram, where the red dashed line indicates the crossover temperature from the semiclassical to the quantum regime of CDFs, determined from $A\log[1/(\tau T)] = M/T$. It shows a significant drop below the doping p_{DMD} [again due to the logarithmic $\gamma(T)$ behavior; in Appendix B, we show that a similar behavior for the resistivity is also obtained when γ diverges logarithmically with the frequency, case (*ii*) in Section 2] and for the parameters given in Figure 3, approaches a small but finite value $M/\gamma \lesssim 1$ K in the doping range between pseudogap and FL region. In the resistivity and doping $p \gtrsim p_{QCR}$ this reflects in the crossover from linear to quadratic behavior as shown in Figure 3c, see also Refs. [32,35,36]. In the pseudogap region, additional scattering mechanisms influence on $\rho(T)$, inducing a decrease from linearity below T^* and an eventual increase at lower temperatures [45–47]. All these further sources of electron scattering, as well as paraconductive fluctuations above the superconducting critical temperature T_c [48,49] are not included within our descriptions, that focus on the

CDF contribution only, under experimental conditions that suppress the other scattering channels. One may argue that the energy scales related to other scattering mechanisms (e.g., T^* or T_c) would eventually appear as low-energy cutoffs in Equation (4), instead of T, preventing γ from diverging. For instance, since superconductivity removes low-energy fermion quasiparticles, the damping γ is expected to *decrease* when entering the superconducting phase (see Section 5).
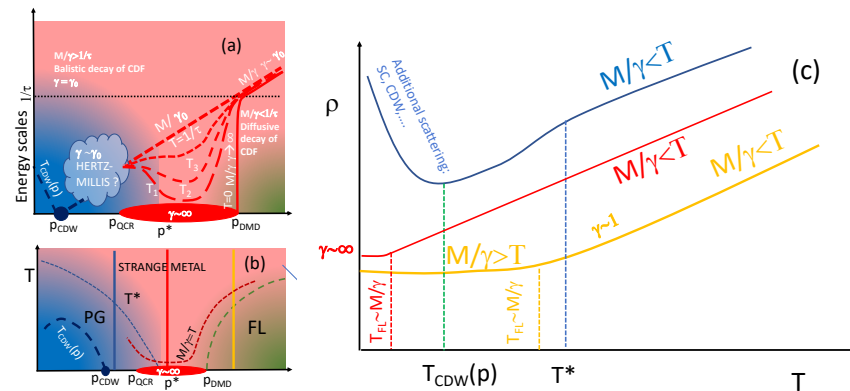
Figure 3. (**a**) Schematic representation of the energy scales and their evolution with doping and temperature. The green shaded area corresponds to the Fermi liquid region of the phase diagram [see panel (**b**)], the blue region is where the pseudogap is present, while in the reddish region, the strange metal occurs. The dark blue dashed lines separate the standard renormalized classical, quantum critical, and quantum disordered regions around the true CDW-QCP. The red dashed line mark the doping and temperature evolution of the characteristic energy scale of CDF, M/γ, which decreases substantially when M/γ becomes smaller than $1/\tau$ (dotted black line). In the present scenario, the unknown connection between the large-γ region and the standard Hertz–Millis QCP is represented by a question mark in a cloud. (**b**) Schematic phase diagram of cuprates as a function of doping p reporting the pseudogap crossover temperature T^* (blue short-dashed line), the hidden transition line $T_{CDW}(p)$ for charge density wave formation, ending at $T = 0$ into a CDW-QCP at p_{CDW} is represented by a dark-blue long-dashed line. Below the green dashed line, the Fermi-liquid regime takes place. The red dashed line marks the crossover $M/\gamma = T$ between the semiclassical region of CDF (above it) and the quantum regime (below it). The yellow, red, and blue vertical lines correspond to the resistivity vs. temperature curves reported in (**c**). (**c**) Schematic behavior of the resistivity as a function of T at the doping values corresponding to the regions of the yellow, red, and blue vertical lines of the panel (**b**).

5. Discussion

In this work, we investigated the dynamics of OPF in the disordered region not far from a QCP. Although the quantum OPFs are intrinsically dynamical even at finite temperatures, our results show that a divergent dissipation destroys this quantum character leading to fluctuations that are semiclassical down to $T = 0$. This effect is similar to that found in Ref. [50], where dissipation quenches the instantons describing the quantum tunneling between local free energy minima of a disordered system. The classical statistics induced here by the increase in dissipation is then directly reflected in the linear-in-T resistivity, owing to the almost homogeneous scattering mediated among the Fermi quasiparticles all over the Fermi surface [32,35,36].

A few remarks are now in order. First of all, the ingredients of quenched impurities and 2D short-ranged OPFs are so generic that a similar mechanism can easily be at work in other (maybe all) systems where the strange metal behavior is observed in the form of a linear-in-T resistivity and a logarithmic C_V/T. The heavy fermion systems $CeCu_{6-x}X_x$ (X=Au, Ag) are just possible examples out of many others [2,9,24]. As evident from Equation (4), the logarithmic divergence of term $\delta\gamma$ is a consequence of the fact that we are dealing with a 2D system. Strictly speaking, the possible divergence of $\delta\gamma$, as well as

the low-temperature trend, depends crucially on this assumption. The extension to 3D (anisotropic) systems would, in principle, introduce a temperature scale Θ_{3D} below which the 3D behavior is recovered and the logarithmic divergence of γ stops. The question that remains open is whether the scale Θ_{3D} can be effectively suppressed along with the increase of the relaxation time of the OPFs, which seems to be a necessary condition to observe the strange metal behavior down to low temperatures in 3D systems.

The proximity to a QCP (charge density waves for cuprates, antiferromagnetic for heavy fermions) easily accounts for the observation of scaling properties. Our guess, within our scenario, is that scaling, being based on a large, diverging ξ, is truly observed at the QCP [24], while the true strange metal behavior (with linear-in-T resistivity) should occur away from it, where M/γ is small or vanishing but ξ is finite and still rather short. This mismatch between the precise tuning of $x = x_c$ to observe scaling properties and bona-fide criticality at the QCP and the (possibly extended) range of strange metal behavior at $x_{\mathrm{QCR}} < x < x_{\mathrm{DMD}}$ (with $x_{\mathrm{QCR}} > x_c$) is a definite testable prediction of our scenario, which calls for more precise experimental scrutiny (actually, this is the case in the $YBa_2Cu_3O_y$ cuprates, where $p_c = p_{\mathrm{CDW}} = 0.16$, while strange metal properties are observed around $p^* \approx 0.19$ [29]). Concerning cuprates, another intriguing, so far unsolved, issue concerns the effect of pseudogap and superconductivity on the dissipation parameter γ. Since this latter is naturally related to the density of states of particles near the Fermi surface (both in the ballistic and the diffusive regimes), we argue that pseudogap and superconductivity should induce a decrease of γ, thereby opposing the strange metal behavior, as indeed observed below T^*.

Another prediction of our scenario is related to the $M/\gamma = 1/\tau$ condition setting the doping regime where diffusion leads to an increasing γ. Thus far, in the paper, the condition is governed by varying M (i.e., ξ) when approaching x_c at a fixed $1/\tau$. We suggest that an increase in disorder (e.g., by ion irradiation) might increase the elastic scattering rate $1/\tau$ extending the range in T and p where strange metal properties are observed. On the other hand, for quasi-2D systems characterized by a relatively small scattering rate $1/\tau$, the interval of doping where the strange metal behavior is observed down to very low temperature, according to our scenario, should become very narrow. Therefore, another possible test for our theory could be to examine particularly clean 2D systems.

A final remark is that the divergence of γ at $T = 0$ marks a complete slowing down of the OPFs, which acquires a vanishing characteristic energy. Considering an ensemble of OPFs that freeze when $\gamma \to \infty$, one might speculate that some kind of glassy state of frozen short-ranged OPFs might occur at $T = 0$ over an extended range of x slightly above a 2D QCP. This is another intriguing testable consequence of our scenario.

Author Contributions: Conceptualization, M.G., C.D.C., G.S. and S.C.; methodology, M.G., C.D.C., G.S. and S.C.; software, G.M.; validation, M.G., C.D.C., G.S. and S.C.; formal analysis, M.G., C.D.C., G.M., G.S. and S.C.; investigation, M.G., C.D.C., G.M., G.S. and S.C.; writing—original draft preparation, M.G., C.D.C., G.S. and S.C.; writing—review and editing, M.G., C.D.C., G.M., G.S. and S.C.; supervision, S.C.; funding acquisition, M.G., G.S. and S.C. All authors have read and agreed to the published version of the manuscript.

Data Availability Statement: No new data were created, except for those that represent the numerical calculations of our main formulas, which were obtained using a C++ code written by one of the authors (G.M.).

Conflicts of Interest: The authors declare no conflict of interest.

Appendix A. Specific Heat in the Presence of a Damping That Is Logarithmically Divergent in $|\omega_n|$

If the damping acquires a logarithmic divergence in the Matsubara frequency, case (*ii*) and Equation (6) in Section 2, the propagator of the collective mode is

$$\mathcal{D}(\omega, q) = \frac{1}{M_q - i\left(\gamma_0 + A\log\sqrt{1 + \frac{\Lambda_{max}^2}{\omega^2}}\right)\omega + A\,\omega\arctan\left(\frac{\Lambda_{max}}{\omega}\right) - \frac{\omega^2}{\overline{\Omega}}},$$

where $M_q = M + \nu(q - q_c)^2$, $M \propto \xi^{-2}$ measures the distance from criticality and $\overline{\Omega}$ is a high-frequency cutoff. Following the calculations of Refs. [35,36], one obtains for the specific heat C_V the following relation:

$$\frac{C_V}{T} = \frac{k_B^2}{2}\int_{-\infty}^{\infty}\beta e^{\beta\omega}\left(\frac{\beta\omega}{e^{\beta\omega} - 1}\right)^2 \rho_b(\omega)\,d\omega, \tag{A1}$$

where we kept the explicit dependence on the Boltzmann constant k_B, so that $\beta = (k_B T)^{-1}$,

$$\rho_b(\omega) = \frac{1}{\pi^2\nu}\left[k_1\log\sqrt{\frac{(\mathcal{A} + \pi\nu)^2 + \mathcal{B}^2}{\mathcal{A}^2 + \mathcal{B}^2}} + k_2\left(\arctan\left(\frac{\mathcal{A} + \pi\nu}{\mathcal{B}}\right) - \arctan\left(\frac{\mathcal{A}}{\mathcal{B}}\right)\right)\right]$$

$$\simeq \frac{1}{\pi^2\nu}\left(\gamma_0 + A\log\frac{\Lambda_{max}}{\omega}\right)\log\left(1 + \frac{\pi\nu}{M}\right), \qquad \text{when } \omega \to 0$$

is an effective density of states, which takes into account the self-energy corrections to the propagator of the collective mode, and

$$\mathcal{A} \equiv M + A\,\omega\arctan\left(\frac{\Lambda_{max}}{\omega}\right) - \frac{\omega^2}{\overline{\Omega}}, \qquad \mathcal{B} \equiv \left(\gamma_0 + A\log\sqrt{1 + \frac{\Lambda_{max}^2}{\omega^2}}\right)\omega,$$

$$k_1 \equiv \gamma_0 + A\log\sqrt{1 + \frac{\Lambda_{max}^2}{\omega^2}} - A\frac{\Lambda_{max}^2}{\Lambda_{max}^2 + \omega^2},$$

$$k_2 \equiv \frac{2\omega}{\overline{\Omega}} - A\arctan\left(\frac{\Lambda_{max}}{\omega}\right) + A\frac{\omega\Lambda_{max}}{\Lambda_{max}^2 + \omega^2}.$$

Notice that k_1 is logarithmically divergent in the limit $\omega \to 0$, unless we set Λ_{max} and/or A is identically equal to zero. All other terms are regular in this limit. The asymptotic expression for Equation (A1) is, therefore,

$$\frac{C_V}{T} \simeq \frac{k_B^2}{3\nu}\left(\gamma_0 + A\log\frac{\Lambda_{max}}{k_B T}\right)\log\left(1 + \frac{\pi\nu}{M}\right).$$

The behavior of this expression is shown in Figure A1, together with the experimental data for $La_{1.36}Nd_{0.4}Sr_{0.24}CuO_4$, taken from Ref. [10].
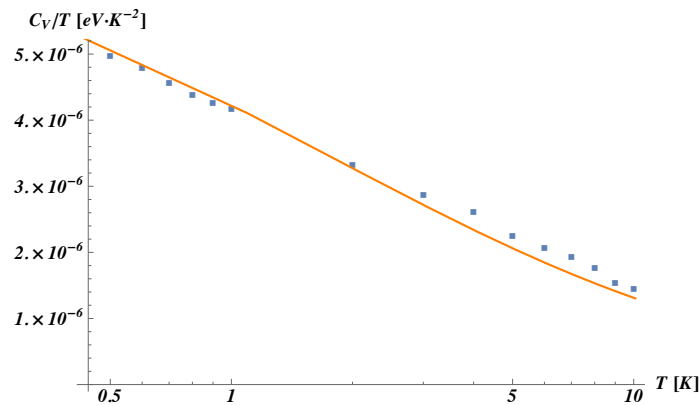
Figure A1. Plot of the specific heat ratio C_V/T as a function of temperature (solid line). Parameter values are $M = 15\,\mathrm{meV}$, $v = 1.3\,\mathrm{eV/(r.l.u.)^2}$, $\overline{\Omega} = 30\,\mathrm{meV}$, $A = 6.5$, $\gamma = 5.5$, $g = 245\,\mathrm{meV}$, $\Sigma_0 = 16\,\mathrm{meV}$, and $q_c = 1.95$ r.l.u. The symbols (squares) represent the experimental values for $\mathrm{La_{1.36}Nd_{0.4}Sr_{0.24}CuO_4}$, taken from Ref. [10]. Similarly to Refs. [35,36], the theoretical specific heat overestimates the experimental data by a constant factor, here equal to 43, presumably due to to the fact that CDFs occupy a fraction of the system and define a sparser effective lattice of their own.

Appendix B. Resistivity in the Presence of a Damping That Is Logarithmically Divergent in $|\omega_n|$

The imaginary part of the electron self-energy for our system (within the Fock approximation) is given by [51]

$$\mathrm{Im}\,\Sigma_{el}(\omega, k) = \frac{\tilde{g}^2}{N}\sum_p \mathrm{Im}\,\mathcal{D}(\omega - \xi_{k-p}, p)\Big[f(\xi_{k-p}) + b(\xi_{k-p} - \omega)\Big], \tag{A2}$$

where $\tilde{g}$ is the coupling between electrons and CDFs, ξ_k is the band dispersion law of the electrons with respect to the chemical potential, $f(z) = [e^{\beta z} + 1]^{-1}$ is the Fermi function, and $b(z) = [e^{\beta z} - 1]^{-1}$ is the Bose function. The real part of Σ is obtained by Kramers–Kronig transformation and the electron Green function is $G = (\omega - \xi_k - \Sigma_{el})^{-1}$. Notice that the coupling constant $\tilde{g}$ which appears in this expression is not the coupling constant g which describes the coupling of the CDFs with diffusive modes. In principle, the self-energy is momentum-dependent, nevertheless, it is a good approximation to consider $\Sigma_{el}(\omega, k) \simeq \Sigma_{el}(\omega)$ [32]. The reason is that CDFs are very broad in momentum space, so they mediate an essentially isotropic interaction. To mimic scattering mediated by quenched impurities, we will always apply the following substitution:

$$|\mathrm{Im}\,\Sigma_{el}(\omega)| \to |\mathrm{Im}\,\Sigma_{el}(\omega)| + \Gamma_0, \tag{A3}$$

where Γ_0 is a positive constant term that has the dimension of energy. It is linked to the average scattering time τ due to quenched impurities by the relation $2\tau = 1/\Gamma_0$.

We compute the resistivity using Kubo formula [32] and find

$$\rho = \left[e^2 \int_{-\infty}^{+\infty}\left[\frac{1}{N}\sum_{k,\sigma}\frac{1}{2}|v_k|^2\mathrm{Im}\,G(\omega, \xi_k)^2\right]\left(-\frac{\partial f(\omega)}{\partial \omega}\right)\frac{\mathrm{d}\omega}{\pi}\right]^{-1},$$

where $v_k = \partial_k \xi_k$ is the group velocity of an electron. The sum over k, which appears in the expression of ρ, can be performed using the Allen approximation [52]

$$\rho = \left[2e^2\widetilde{N}(0)\int_{-\infty}^{+\infty}\left[\int_{-\infty}^{+\infty}\mathrm{Im}\,G(\omega, \xi)^2\frac{\mathrm{d}\xi}{\pi}\right]\left(-\frac{\partial f(\omega)}{\partial \omega}\right)\mathrm{d}\omega\right]^{-1},$$

$$\widetilde{N}(\xi) \equiv \frac{1}{N}\sum_k\frac{1}{2}|v_k|^2\delta(\xi - \xi_k) = \frac{1}{N}\sum_k\frac{\partial^2\xi_k}{\partial k_x^2}\theta(\xi - \xi_k). \tag{A4}$$

Notice that the overall factor 2 is due to the spin multiplicity of the electrons. The integral in $d\xi$ can now be solved analytically. The resulting expression for the resistivity is

$$\rho = \left[e^2 \widetilde{N}(0) \int_{-\infty}^{+\infty} \frac{1}{|\mathrm{Im}\, \Sigma_{el}(\omega, T)|} \left(-\frac{\partial f(\omega)}{\partial \omega} \right) d\omega \right]^{-1},$$

which, in the $T \to 0$ limit, reduces to

$$\rho = \frac{\Gamma_0}{e^2 \widetilde{N}(0)},$$

namely, the reciprocal of the product between $\widetilde{N}(0)$ (which encodes all the information about the currents, except for the spin) and twice the zero temperature scattering time τ. The behavior of this expression is shown in Figure A2, together with the experimental data for $La_{1.36}Nd_{0.4}Sr_{0.24}CuO_4$, taken from Ref. [10].
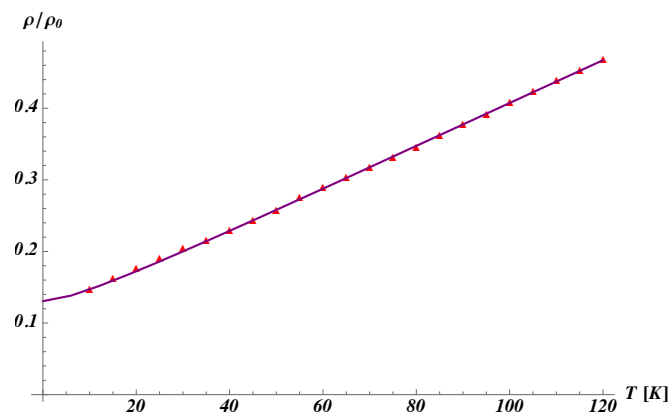

Figure A2. Plot of the resistivity as a function of temperature (solid line). Parameter values are $M = 15\,\mathrm{meV}$, $\nu = 1.3\,\mathrm{eV/(r.l.u.)^2}$, $\overline{\Omega} = 30\,\mathrm{meV}$, $A = 6.5$, $\gamma = 5.5$, $g = 245\,\mathrm{meV}$, $\Gamma_0 = 16\,\mathrm{meV}$ and $q_C = 1.95$ r.l.u. The symbols (triangles) represent the experimental values for $La_{1.36}Nd_{0.4}Sr_{0.24}CuO_4$, taken from Ref. [10]. We use the notation $\rho_0 = \hbar a/e^2$.

References

1. Varma, C.M.; Nussinov, Z.; van Saarloss, W. Singular or non-Fermi liquids. *Phys. Rep.* **2002**, *361*, 267. [CrossRef]
2. Stewart, G.R. Non-Fermi-liquid behavior in *d*- and *f*-electron metals. *Rev. Mod. Phys.* **2001**, *73*, 797. [CrossRef]
3. Bruin, J.A.N.; Sakai, H.; Perry, R.S.; Mackenzie, A.P. Similarity of scattering rates in metals showing $T-$linear resistivity. *Science* **2013**, *339*, 804. [CrossRef] [PubMed]
4. Taupin, M.; Paschen, S. Are heavy fermion strange metals Planckian? *Crystals* **2022**, *12*, 251. [CrossRef] [PubMed]
5. Legros, A.; Benhabib, S.; Tabis, W.; Laliberté, F.; Dion, M.; Lizaire, M.; Vignolle, B.; Vignolles, D.; Raffy, H.; Li, Z.Z.; et al. Universal $T-$linear resistivity and Planckian dissipation in overdoped cuprates. *Nat. Phys.* **2019**, *15*, 142. [CrossRef]
6. Greene, R.L.; Mandal, P.R.; Poniatowski, N.R.; Sarka, T. The strange metal state of the electron-doped cuprates. *Annu. Rev. Condens. Matter Phys.* **2020**, *11*, 213. [CrossRef]
7. Walmsley, P.; Putzke, C.; Malone, L.; Guillamón, I.; Vignolles, D.; Proust, C.; Badoux, S.; Coldea, A.I.; Watson, M.D.; Kasahara, S.; et al. Quasiparticle mass enhancement close to the quantum critical point in $BaFe_2(As_{1-x}P_x)_2$. *Phys. Rev. Lett.* **2013**, *110*, 257002. [CrossRef]
8. Cao, Y.; Chowdhury, D.; Rodan-Legrain, D.; Rubies-Bigorda, O.; Watanabe, K.; Taniguchi, T.; Senthil, T.; Jarillo-Herrero, P. Strange metal in magic-angle graphene with near Planckian dissipation. *Phys. Rev. Lett.* **2020**, *124*, 076801. [CrossRef]
9. Stockert, O.; Löhneysen, H.v.; Rosch, A.; Pyka, N.; Loewenhaupt, M. Two-Dimensional Fluctuations at the quantum-critical point of $CeCu_{6-x}Au_x$. *Phys. Rev. Lett.* **1998**, *80*, 5627. [CrossRef]
10. Michon, B.; Girod, C.; Badoux, S.; Kamarík, J.; Ma, Q.; Dragomir, M.; Dabkowska, H.A.; Gaulin, B.D.; Zhou, J.-S.; Pyon, S.; et al. Thermodynamic signatures of quantum criticality in cuprate superconductors. *Nature* **2019**, *567*, 218222. [CrossRef]
11. Anderson, P.W. *The Theory of Superconductivity in the High Temperature Cuprates*; Princeton University Press: Princeton, NJ, USA, 1997.
12. Kastrinakis, G. A Fermi liquid model for the overdoped and optimally doped cuprate superconductors: Scattering rate, susceptibility, spin resonance peak and superconducting transition. *Physica C* **2000**, *340*, 119. [CrossRef]

13. Faulkner, T.; Iqbal, N.; Liu, H.; McGreevy, J.; Vegh, D. Strange metal transport realized by gauge/gravity duality. *Science* **2010**, *329*, 1043. [CrossRef] [PubMed]

14. Hartnoll, S.A. Theory of universal incoherent metallic transport. *Nat. Phys.* **2015**, *11*, 54. [CrossRef]

15. Patel, A.A.; McGreevy, J.; Arovas, D.P.; Sachdev, S. Magnetotransport in a model of a disordered strange metal. *Phys. Rev. X* **2018**, *8*, 021049. [CrossRef]

16. Castellani, C.; Di Castro, C.; Metzner, W. Dimensional crossover from Fermi to Luttinger liquid. *Phys. Rev. Lett.* **1994**, *72*, 316. [CrossRef]

17. Abanov, A.; Chubukov, A.; Schmalian, J. Quantum-critical theory of the spin-fermion model and its application to cuprates: Normal state analysis. *Adv. Phys.* **2003**, *52*, 11. [CrossRef]

18. Rosch, A. Interplay of disorder and spin fluctuations in the resistivity near a quantum critical point. *Phys. Rev. Lett.* **1999**, *82*, 4280. [CrossRef]

19. Zhang, S.-S.; Berg, E.; Chubukov, A.V. Free energy and specific heat near a quantum critical point of a metal. *arXiv* **2023**, arXiv:2301.01873v1.

20. Castellani, C.; Di Castro, C.; Grilli, M. Singular quasiparticle scattering in the proximity of charge instabilities. *Phys. Rev. Lett.* **1995**, *75*, 4650. [CrossRef]

21. Metzner, W.; Rohe, D.; Andergassen, S. Soft Fermi surfaces and breakdown of Fermi-liquid behavior. *Phys. Rev. Lett.* **2003**, *91*, 066402. [CrossRef]

22. Varma, C.M. Colloquium: Linear in temperature resistivity and associated mysteries including high temperature superconductivity. *Rev. Mod. Phys.* **2020**, *92*, 031001. [CrossRef]

23. Si, Q. The local quantum critical point and non-Fermi liquid properties. *J. Phys. Condens. Matter* **2003**, *15*, S2207–S2213. [CrossRef]

24. Schröder, A.; Aeppli, G.; Coldea, R.; Adams, M.; Stockert, O.; Löhneysen, H.V.; Bucher, E.; Ramazashvili, R.; Coleman, P. Onset of antiferromagnetism in heavy-fermion metals. *Nature* **2000**, *407*, 351. [CrossRef] [PubMed]

25. Dumitrescu, P.T.; Wentzell, N.; Georges, A.; Parcollet, O. Planckian metal at a doping-induced quantum critical point. *Phys. Rev. B* **2022**, *105*, L180404. [CrossRef]

26. Andergassen, S.; Caprara, S.; Di Castro, C.; Grilli, M. Anomalous isotopic effect near the charge-ordering quantum criticality. *Phys. Rev. Lett.* **2001**, *87*, 056401. [CrossRef]

27. Caprara, S.; Di Castro, C.; Seibold, G.; Grilli, M. Dynamical charge density waves rule the phase diagram of cuprates. *Phys. Rev. B* **2017**, *95*, 224511. [CrossRef]

28. Caprara, S. The ancient Romans' route to charge density waves in cuprates. *Condens. Matter* **2019**, *4*, 60. [CrossRef]

29. Badoux, S.; Tabis, W.; Laliberté, F.; Grissonnanche, G.; Vignolle, B.; Vignolles, D.; Bárd, J.; Bonn, D.A.; Hardy, W.N.; Liang, R.; et al. Change of carrier density at the pseudogap critical point of a cuprate superconductor. *Nature* **2016**, *531*, 210. [CrossRef]

30. Arpaia, R.; Caprara, S.; Fumagalli, R.; Vecchi, G.D.; Peng, Y.Y.; Andersson, E.; Betto, D.; Luca, G.M.D.; Brookes, N.B.; Lombardi, F.; et al. Dynamical charge density fluctuations pervading the phase diagram of a Cu-based high$-T_c$ superconductor. *Science* **2019**, *365*, 906–910. [CrossRef]

31. Di Castro, C. Revival of charge density waves and charge density fluctuations in cuprate high-temperature superconductors. *Condens. Matter* **2020**, *5*, 70. [CrossRef]

32. Seibold, G.; Arpaia, R.; Peng, Y.Y.; Fumagalli, R.; Braicovich, L.; Di Castro, C.; Grilli, M.; Ghiringhelli, G.; Caprara, S. Strange metal behaviour from charge density fluctuations in cuprates. *Commun. Phys.* **2021**, *4*, 7. [CrossRef]

33. Varma, C.M.; Littlewood, P.B.; Schmitt-Rink, S.; Abrahams, E.; Ruckenstein, A.E. Phenomenology of the normal state of Cu-O high-temperature superconductors. *Phys. Rev. Lett.* **1989**, *63*, 1996. [CrossRef]

34. Hlubina, R.; Rice, T.M. Resistivity as a function of temperature for models with hot spots on the Fermi surface. *Phys. Rev. B* **1995**, *51*, 9253. [CrossRef] [PubMed]

35. Caprara, S.; Di Castro, C.; Mirarchi, G.; Seibold, G.; Grilli, M. Dissipation-driven strange metal behavior. *Commun. Phys.* **2022**, *5*, 10. [CrossRef]

36. Mirarchi, G.; Seibold, G.; Di Castro, C.; Grilli, M.; Caprara, S. The strange-metal behavior of cuprates. *Condens. Matter* **2022**, *7*, 29. [CrossRef]

37. Di Castro, C.; Raimondi, R. *Statistical Mechanics and Applications in Condensed Matter*; Cambridge University Press: Cambridge, UK, 2015.

38. Hertz, J.A. Quantum critical phenomena. *Phys. Rev. B* **1976**, *14*, 1165. [CrossRef]

39. Millis, A.J. Effect of a nonzero temperature on quantum critical points in itinerant fermion systems. *Phys. Rev. B* **1993**, *48*, 7183. [CrossRef] [PubMed]

40. Girod, C.; LeBoeuf, D.; Demuer, A.; Seyfarth, G.; Imajo, S.; Kindo, K.; Kohama, Y.; Lizaire, M.; Legros, A.; Gourgout, A.; et al. Normal state specific heat in the cuprate superconductors $La_{2-x}Sr_xCuO_4$ and $Bi_{2+y}Sr_{2-x-y}La_xCuO_{6+\delta}$ near the critical point of the pseudogap phase. *Phys. Rev. B* **2021**, *103*, 214506. [CrossRef]

41. Momono, N.; Ido, M.; Nakano, T.; Oda, M.; Okajima, Y.; Yamaya, K. Low-temperature electronic specific heat of $La_{2-x}Sr_xCuO_4$ and $La_{2-x}Sr_xCu_{1-y}Zn_yO_4$. Evidence for a d wave superconductor. *Physica C* **1994**, *233*, 395. [CrossRef]

42. Pfleiderer, C.; Böni, P.; Keller, T.; ler, U.K.R.; Rosch, A. Non-Fermi liquid metal without quantum criticality. *Science* **2007**, *316*, 1871. [CrossRef]

43. Ayres, J.; Berben, M.; Čulo, M.; Hsu, Y.-T.; van Heumen, E.; Huang, Y.; Zaanen, J.; Kondo, T.; Takeuchi, T.; Cooper, J.R.; et al. Incoherent transport across the strange-metal regime of overdoped cuprates. *Nature* **2021**, *595*, 661. [CrossRef] [PubMed]

44. Hussey, N.E.; Duffy, C. Strange metallicity and high$-T_c$ superconductivity: Quantifying the paradigm. *Sci. Bull.* **2022**, *67*, 985-987. [CrossRef] [PubMed]

45. Boebinger, G.S.; Ando, Y.; Passner, A.; Kimura, T.; Okuya, M.; Shimoyama, J.; Kishio, K.; Tamasaku, K.; Ichikawa, N.; Uchida, S. Insulator-to-metal crossover in the normal state of $La_{2-x}Sr_xCuO_4$ near optimum doping. *Phys. Rev. Lett.* **1996**, *77*, 5417. [CrossRef] [PubMed]

46. Ando, Y.; Komiya, S.; Segawa, K.; Ono, S.; Kurita, Y. Electronic phase diagram of high$-T_c$ cuprate superconductors from a mapping of the in-llane resistivity curvature. *Phys. Rev. Lett.* **2004**, *93*, 267001. [CrossRef]

47. Wahlberg, E.; Arpaia, R.; Seibold, G.; Rossi, M.; Fumagalli, R.; Trabaldo, E.; Brookes, N.B.; Braicovich, L.; Caprara, S.; Gran, U.; et al. Restored strange metal phase through suppression of charge density waves in underdoped $YBa_2Cu_3O_{7-\delta}$. *Science* **2021**, *373*, 1506–1510. [CrossRef] [PubMed]

48. Caprara, S.; Grilli, M.; Leridon, B.; Lesueur, J. Extended paraconductivity regime in underdoped cuprates. *Phys. Rev. B* **2005**, *72*, 104509. [CrossRef]

49. Caprara, S.; Grilli, M.; Leridon, B.; Vanacken, J. Paraconductivity in layered cuprates behaves as if due to pairing of nearly free quasiparticles. *Phys. Rev. B* **2009**, *79*, 024506. [CrossRef]

50. Millis, A.J.; Morr, D.K.; Schmalian, J. Quantum Griffiths effects in metallic systems. *Phys. Rev. B* **2002**, *66*, 174433.

51. Mazza, G.; Grilli, M.; Di Castro, C.; Caprara, S. Evidence for phonon-like charge and spin fluctuations from an analysis of angle-resolved photoemission spectra of $La_{2-x}Sr_xCuO_4$ superconductors. *Phys. Rev. B* **2013**, *87*, 014511. [CrossRef]

52. Allen, P.B. Electron self-energy and generalized Drude formula for infrared conductivity of metals. *Phys. Rev. B* **2015**, *92*, 054305. [CrossRef]